

Article

Evaluation of the Thickness and Oxygen Transmission Rate before and after Thermoforming Mono- and Multi-layer Sheets into Trays with Variable Depth

Mieke Buntinx ^{1,*}, Gert Willems ¹, Griet Knockaert ¹, Dimitri Adons ¹, Jan Yperman ², Robert Carleer ² and Roos Peeters ¹

¹ Research Group Packaging Center, Institute for Materials Research–Institute for Materials Research in Microelectronics (IMO–IMOMEC), University Hasselt, Wetenschapspark 27, 3590 Diepenbeek, Belgium; E-Mails: gert.willems@uhasselt.be (G.W.); griet.knockaert@uhasselt.be (G.K.); dimitri.adons@uhasselt.be (D.A.); roos.peeters@uhasselt.be (R.P.)

² Research Group Applied and Analytical Chemistry, Institute for Materials Research–Institute for Materials Research in Microelectronics (IMO–IMOMEC)/Centre for Environmental Sciences (CMK), University Hasselt, Agoralaan building D, 3590 Diepenbeek, Belgium; E-Mails: jan.yperman@uhasselt.be (J.Y.); robert.carleer@uhasselt.be (R.C.)

* Author to whom correspondence should be addressed; E-Mail: mieke.buntinx@uhasselt.be; Tel.: +32-11-292-155.

External Editor: Taek-Soo Kim

Received: 22 September 2014; in revised form: 6 December 2014 / Accepted: 12 December 2014 / Published: 22 December 2014

Abstract: During thermoforming, plastic sheets are heated and subsequently deformed through the application of mechanical stretching and/or pressure. This process directly impacts sheet properties such as material thickness in walls, corners, and bottom, crystallinity in the constituent layers, and particularly the oxygen gas permeability. The aim of this study was to quantify the impact of thermoforming on thickness and oxygen transmission rate (OTR) of selected packaging materials (polypropylene (PP); PP/ethylene-vinyl alcohol co-polymer/PP (PP/EVOH/PP); polystyrene/EVOH/polyethylene (PS/EVOH/PE); amorphous polyethylene terephthalate/PE (APET/PE); APET/PE/EVOH/PE; polyamide/PE (PA/PE); and (PE/PA/EVOH/PA/PE). These materials were extruded in two different thicknesses and thermoformed into trays with the same top dimensions and variable depths of 25, 50, and/or 75 mm and a 50 mm tray with a variable radius of the corners. The distribution of the material thickness in the trays was visualized, showing the

locations that were most affected by the deep drawn process. The OTR results indicate that the calculated OTR, based on a homogeneous material distribution, can be used as a rough approximation of the measured OTR. However, detailed analysis of crystallization and unequal thinning, which is also related to the tray design, remains necessary to explain the deviation of the measured OTR as compared to the predicted one.

Keywords: thermoforming; oxygen transmission rate; gas barrier; EVOH; semi-rigid food packaging; flexible food packaging film

1. Introduction

Thermoformed trays are widely used to package prepared meals, fresh or frozen products, and other foods [1]. During the thermoforming process, an (inline) extruded film or sheet is heated to its softening temperature and subsequently deformed through application of mechanical stretching and/or pressure into a tray. The design of the tray is defined by the mold. This process directly impacts several properties of the sheet material, such as thickness in walls, corners and bottom, crystallinity of the constituent layers, mechanical and optical properties and particularly the gas permeability. Cooling e.g., is essential to avoid shrinkage after production [2,3].

An important characteristic of food packaging, especially in the case of modified atmosphere packaging (MAP), is the oxygen permeability. The food and packaging industry has a strong interest in the specification of the barrier properties of the thermoformed tray, based on the oxygen transmission rate (OTR) and thickness of the sheet or film. As a result of the increased surface area and thinning of the sheet, the OTR of the tray will increase. However, various studies have shown that the OTR of the sheet material cannot easily be extrapolated to thermoformed packaging [4–6]. One of the reasons might be a poor control of the material thickness distribution in the walls, the corners, and/or the bottom, which is a major drawback of thermoforming [7–9]. On the other hand, the effect of physical thinning on the OTR can be partially neutralized by reorientation, closer chain packaging, and restriction of chain mobility of polymer chains in the amorphous zones during deep drawing and stretching of the material [10]. Reorientation and crystallization are related to altered sorption and diffusion of oxygen in polymer materials, and might cause a decrease of the OTR [11].

Non-uniform wall thickness distribution is caused by differential stretching during the thermoforming process. However, some improvement in wall thickness uniformity can be achieved by mechanical stretching of the heated sheet prior to bringing it into contact with the mold surface using a mechanical plug [2,7,12]. Various studies have been conducted to assess the effect of processing parameters, such as mold temperature, film temperature, plug velocity, plug holding time, and plug clearance, on the wall thickness distribution. These parameters are strongly related to the thermoforming window of the tested polymers [12–15]. Amorphous polymers, such as polystyrene (PS), can be shaped with relative ease above their glass transition temperature and generally exhibit relative wide thermoforming windows [2,12], whereas semi-crystalline polymers, such as homopolymer polypropylene (PP), are more difficult to thermoform because they are so fluid above melting temperature that they must be processed within a narrow temperature range around the crystalline

melting point [2,14,15]. Furthermore, the optimization of the thermoforming process is even more complicated when a combination of polymers within a multilayer structure is processed, e.g., ethylene-vinyl alcohol co-polymer (EVOH) coextruded as an internal layer within PP, PS, polyethylene (PE), amorphous polyethylene terephthalate (APET), and/or polyamide (PA) layers [15]. When thermoforming light-gauge multilayer barrier sheet materials such as PP/EVOH/PP, PS/EVOH/PE, APET/PE/EVOH/PE, or PA/EVOH/PA/PE into packaging, care must be taken to ensure that the barrier layer (EVOH) remains thick enough in the thinnest portion of the formed container to maintain sufficient gas barrier properties [2,16]. In addition to traditional trial and error methods for product and process development, researchers have made significant advances in the simulation of thermoforming processing techniques. O'Connor *et al.* have summarized experiments and test equipment that are able to simulate polymer behavior during thermoforming [14]. From these experimental test results, finite element analysis programs can be developed to model a wide range of mold geometries and polymer processing techniques, to predict and optimize the material distribution in a part prior to any thermoforming process [10,14,15].

From this perspective, the MaProDe_Ox project was conducted in collaboration with companies from the Belgian food and packaging industry. The aim was to evaluate the thickness and OTR of selected commercial packaging materials before and after thermoforming into trays with variable depth (25, 50, and/or 75 mm) and a variation of the radius of the corners in the 50-mm trays. This paper reports on the results of five semi-rigid thin-gauge sheets and two flexible films. All materials, except APET/PE/EVOH/PE, were extruded in two different thicknesses that are commonly used in food packaging.

2. Experimental Section

2.1. Sheets and Trays

The selected sheet materials were provided by Cobelplast (Lokeren, Belgium) and EuralPack (Schoten, Belgium). The high barrier multilayers consisted of ~3% EVOH (EVAL™, Kuraray, EVAL Europe, Zwijndrecht, Belgium). All EVOH types were suitable for thermoforming applications and contained 32 mol% ethylene. Only the PA multilayers consisted of ~4% EVOH, with the 300- μm PE/PA/EVOH/PA/PE sheet containing a 38 mol% ethylene EVOH type. All sheet materials are listed in Table 1.

The thermoforming equipment used was a custom-made lab thermoformer able to simulate industrial thermoforming processes from Cobelplast (Lokeren, Belgium). Sheets with a maximum size of 250 mm \times 330 mm were pre-heated using contact heat (2×2 plates), and deep drawn in a water cooled single mold cavity, using compressed air and a plug. The mold cavity was suitable for containers with top dimensions of 190 mm \times 132 mm, a conicity of 10 in the side walls and a variable depth of maximal 100 mm. Using four different inserts in the mold, the materials were thermoformed into trays with variable depths of 25, 50, and/or 75 mm (corners with radius ~ 1 mm), and a variant of the 50-mm tray with round corners (radius 5 mm). The different tray types will be abbreviated respectively as 25, 50, 75, and 50/R5. The plug had top dimensions of 182 mm \times 124 mm, a height of 85 mm, and a conicity of 10°, and the radius of its corners in the bottom was 5 mm. The plug was made of Hytac-FLXT (CMT Materials, Attleboro, MA, USA), consisting of syntactic composite foam with a Teflon coating.

As syntactic foam has a low conductivity, it prevents heat loss from the sheet to the plug. The Teflon coating lowers the coefficient of friction of the plug, allowing the sheet to slide more easily over the plug [2,7]. The plug was not used for thermoforming the four flexible PA films, nor for the 25-mm trays from PP and PP/EVOH/PP sheets. In addition, a plug with more rounded corners (radius 20 mm) was used for thermoforming the thicker PP and PP/EVOH/PP sheets. Processing parameters such as cycle speed, amounts of heating runs, and timing of the plug movement and compressed air were optimized according to extensive industrial experience. The bottom clearance of the plug was set to 3 cm from the bottom in each tray type. Table 2 shows the plate temperature and number of heating steps that were used for the production of trays that were selected for further thickness and OTR measurements.

Table 1. Sheet materials: suppliers, overall and individual layer thickness, and EVOH%.

Mono- and multi-layers	Sheet supplier	Overall sheet thickness (μm) ¹	Individual layer thickness (μm) ¹	%EVOH
PP	Cobelplast	403 \pm 3	403 \pm 3	-
	Cobelplast	801 \pm 5	801 \pm 5	-
APET/PE	EuralPack	338 \pm 4	288 \pm 3/40 \pm 2	-
	EuralPack	648 \pm 8	596 \pm 5/41 \pm 3	-
PA/PE	EuralPack	166 \pm 2	51 \pm 1/107 \pm 4	-
	EuralPack	293 \pm 5	82 \pm 8/185 \pm 9	-
PP/EVOH */PP	Cobelplast	404 \pm 4	170 \pm 7/13 \pm 1/217 \pm 9	3.2%
	Cobelplast	789 \pm 3	375 \pm 7/24 \pm 2/383 \pm 4	3.0%
PS/EVOH */PE	Cobelplast	413 \pm 3	325 \pm 12/12 \pm 2/41 \pm 8	2.9%
	Cobelplast	817 \pm 3	645 \pm 12/24 \pm 3/77 \pm 8	3.1%
APET/PE/EVOH */PE	EuralPack	369 \pm 3	316 \pm 4/9 \pm 1/10 \pm 1/18 \pm 4	2.7%
PA/EVOH */PA/PE	EuralPack	164 \pm 3	33 \pm 4/8 \pm 1/16 \pm 2/99 \pm 4	4.9%
PE/PA/EVOH */PA/PE	EuralPack	291 \pm 3	83 \pm 1/36 \pm 1/12 \pm 1/54 \pm 1/86 \pm 1	4.1%

¹ mean \pm standard deviation ($n = 10$ locations per film); * EVAL™, Kuraray, EVAL Europe.

Table 2. Overview of processing parameters and formed tray types for each test material.

Mono- and Multi-layers	Overall sheet thickness (μm)	Forming temperatures ($^{\circ}\text{C}$)		Formed tray types
		top/bottom (heating steps)	plate 1	
PP	403 \pm 3	120/120 (3)	154/154 (3)	25, 50/R5, 50
	801 \pm 5	120/120 (2)	158/158 (8)	50/R5, 50, 75
PP/EVOH/PP	404 \pm 4	120/120 (1–3)	154/154 (3–5)	25, 50/R5, 50
	789 \pm 3	120/120 (2)	158/158 (8)	50, 75
PS/EVOH/PE	413 \pm 3	120/120 (1)	140/140 (1)	25, 50/R5, 50
	817 \pm 3	120/120 (2)	140/140 (2)	50, 75
APET/PE	338 \pm 4	80/80 (1)	115/115 (1)	25, 50/R5, 50
	648 \pm 8	80/80 (2)	115/115 (2)	50, 75
APET/PE/EVOH/PE	369 \pm 3	80/80 (1)	105/115 (1)	25, 50/R5, 50
PA/PE	166 \pm 2	60/60 (1)	100/100 (1)	25, 50/R5, 50
	293 \pm 5	115/115 (1)	125/125 (1)	50, 75
PA/EVOH/PA/PE	164 \pm 3	60/60 (1)	110/110 (1)	25, 50/R5, 50
PE/PA/EVOH/PA/PE	291 \pm 3	60/60 (1)	110/110 (2)	50, 75

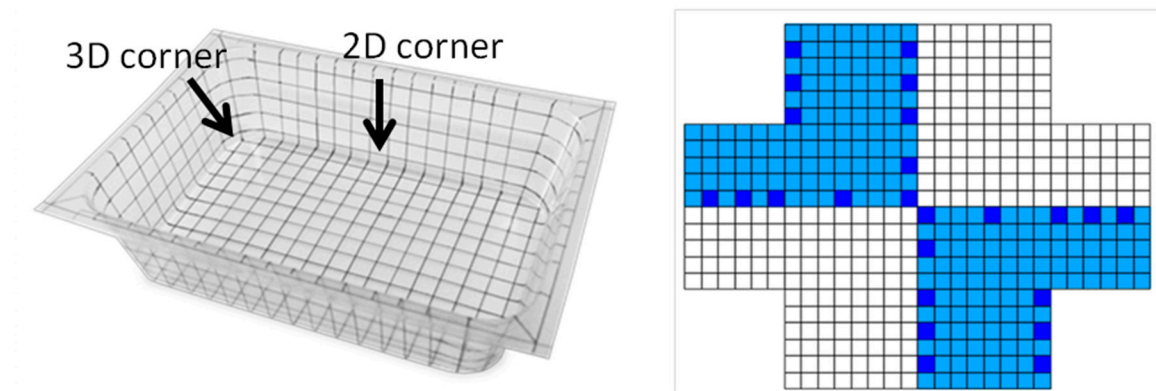
Other processing parameters were optimized for each material according to extensive industrial experience.

2.2. Thickness Measurements

The overall and individual layer thickness in selected locations of the films and trays was determined using a Nikon Eclipse ME600 Microscope equipped with a Nikon DS-Fi2 camera (Nikon, Tokyo, Japan). The overall thickness of the sheets and trays was also measured by means of a handheld thickness gauge (Magna-Mike 8500, Olympus, Tokyo, Japan). All trays were provided with a grid of squares of $\sim 1 \text{ cm}^2$ (Figure 1) and the thickness of the squares was measured. The results are visually presented as percentage thinning, calculated according to Equation (1), with d_0 and d_i representing the thickness of the unconverted sheet and the thickness in square “ i ”, respectively:

$$\text{thinning}_i(\%) = \frac{d_0 - d_i}{d_0} \times 100\% \quad (1)$$

Figure 1. Validation of the global thickness measurements in 236 locations of a 50-mm tray.



2.3. OTR Measurements

The OTR of the sheets was measured using a Mocon Ox-Tran 2/21 (ST or SH module, Minneapolis, MN, USA) in accordance with ASTM (American Society for Testing and Materials) Standard F1927 [17] at 23 °C and controlled relative humidity (RH). Flat sheet samples were clamped into the diffusion cell, which was purged of residual oxygen using an oxygen-free carrier gas. Then pure oxygen (99.9%) was introduced into the outside chamber of the diffusion cell (50% RH) and the oxygen molecules permeating through the film to the inside chamber (90% RH) were conveyed to the sensor by the carrier gas. The OTR was calculated by normalizing the flow rate at a steady state with respect to the oxygen pressure gradient and expressed in $[\text{cc}/\text{m}^2 \cdot \text{day} \cdot \text{atm}]$. All sheets were measured in triplicate.

The OTR of the thermoformed trays was measured using the same equipment in accordance with ASTM Standard F1307 [18] at 23 °C with 50% RH outside and 90% RH inside the package. The topside of the tray was sealed with an impermeable adhesive on a copper plate, which was provided with two small holes for connection to the copper tubing with inflow and outflow of the carrier gas to the Mocon Ox-Tran. The trays were exposed to oxygen from the air and the oxygen permeation was measured from the outside to the inside of the tray. The OTR of the trays is expressed in $[\text{cc}/\text{package} \cdot \text{day} \cdot 0.209 \cdot \text{atm}]$. All trays were measured in duplicate or triplicate.

2.4. Differential Scanning Calorimetry

The mono- and multilayer films were characterized using a Q200 differential scanning calorimeter (DSC, TA Instruments, New Castle, DE, USA). The flat mounted samples (5 mg) were heated at 10 °C/min from 25 to 220 °C or 270 °C and then cooled to 25 °C at 10 °C/min. Subsequently, a second heating run at 10 °C/min to 220 or 270 °C was performed, before finally cooling to 25 °C at 10 °C/min. DSC experiments were also performed on samples from selected locations on the trays. From the DSC curves, the melt enthalpy (ΔH_m) and the degree of crystallinity ($X_c = \Delta H_m / \Delta H_m^0$) of the polymers before and after thermoforming was calculated. All measurements were performed in triplicate under a constant flow of 50 mL/min nitrogen gas.

3. Results and Discussion

3.1. Material Characterization

In order to characterize the test materials, the overall and individual layer thickness was measured microscopically at ten locations per film: five transversal and five perpendicular to the extrusion direction. The results are shown in Table 1 (thin adhesive layers are not shown). From these data, the EVOH content in the multilayers was determined to be on average between 2.7% and 3.2% in the multilayers with PP, PS, and APET, and 4.1% and 4.9% in the multilayers with PA, which was in accordance with the target content.

The chemical composition and thermal features of all polymers in the films were confirmed using DSC analyses (data not shown). The melting temperature of EVOH in the PP/EVOH/PP, PS/EVOH/PE, APET/PE/EVOH/PE, and PA/EVOH/PA/PE multilayers ranged from 180 to 183 °C, indicating an EVOH type with 32 mol% ethylene content [19,20]. The melting temperature of EVOH in the PE/PA/EVOH/PA/PE sheet was 173 °C, indicating an EVOH type with 38 mol% ethylene [19,20].

3.2. Analysis of the Thickness after Thermoforming

The thickness distribution in thermoformed trays is dependent on a variety of processing parameters, such as sheet temperature, mold temperature, heating time, thermoforming pressure, evacuation rate, plug temperature, plug speed, etc. [2,7–9,12,14,21]. To obtain commercially acceptable trays, processing parameters for each material were optimized based on stability and visual criteria of the formed trays. After evaluation by the industrial partners, series of test samples for each tray type were produced for detailed thickness and OTR measurements, and chemical characterization.

Three thermoformed trays of each tray type were provided with a grid of squares of ~1 cm². The percentage thinning in all squares of one 50-mm tray (thick variant of each material) was measured according to Equation 1 and visualized as shown in Figures 2–5 (472 squares in a 50-mm tray). Since the visual presentation of these data showed sufficient symmetry, the thickness of the squares in all other tray types was measured in two diagonal opposing quadrants (197, 236, and 287 squares in the 25-, 50- and 75-mm trays, respectively), and the data were mirrored (Figure 1). To evaluate this method on its reproducibility, 24 strategic locations in the 50-mm trays were selected (Figure 1, dark squares) and the thickness was measured in triplicate on trays thermoformed on two or three

different production times. Analogously, 17 and 29 strategic locations were selected in the 25- and 75-mm trays, respectively. The standard deviation of the thinning% in all selected locations was between 1% and 5%, indicating that the thickness measurements were representative for all trays of the same design. Only the trays produced from flexible PA films showed more deviation, probably due to local shrinkage (standard deviation of 2%–13%).

According to this method, the percentage thinning of each material in the bottom, the walls, and the corners as a consequence of the thermoforming processes was visualized. Figures 2–5 show the results in all tray types thermoformed from the PP, APET/PE, PA/PE, and PS/EVOH/PE sheets, respectively. The initial target thickness of the thin and thicker sheets is shown in Figures 2–5; the measured thickness is shown in Table 1. From these figures, it is clear that the impact on material thinning was increasingly observed in the 25-mm tray, the 50-mm tray with round corners (radius 5), and the 50-mm tray of each material. Furthermore, material thinning in all thin variants was most pronounced in the 3D and the 2D corners in the bottom. In addition, deep drawing of the thicker variants to 50 and 75 mm analogously showed an increasing thinning effect proportional to the depth. However, the locations in the tray that were most affected by the thermoforming process were strongly dependent on the test material, e.g., in the 75-mm trays of PP, the walls were clearly more affected, whereas in the PA/PE trays particularly the bottom was severely thinned. The material distribution in the 75-mm PS/EVOH/PE tray looks more uniform over the walls, corners, and bottom, whereas the pattern in the 75-mm APET/PE tray rather shows an extrapolation of the pattern of the 25- and 50-mm trays. A possible explanation for these differences might be related to the use (or not) of the plug in combination with each test material. Since the plug material is cooler than the softened sheet, the sheet that contacts the plug is chilled and will not stretch as much as the sheet that is free from the plug [2,8,22].

The average thickness \pm standard deviation of all the trays is shown in Table 3. From these data, it can be deduced that the thinning pattern of the PP/EVOH/PP, APET/PE/EVOH/PE, and (PE/PA/EVOH/PA/PE trays was quite similar to the patterns of the PP, APET/PE, and PA/PE trays shown in Figures 2–4, respectively (therefore these patterns are not shown).

Table 3. Average thickness \pm standard deviation of all sheets and trays expressed in μm .

Average thickness (μm)	d_0^{a}	d_{25}^{b}	$d_{50/\text{R5}}^{\text{c}}$	d_{50}^{c}	d_0^{a}	d_{50}^{d}	d_{75}^{e}
PP	403 ± 3	280 ± 59	240 ± 81	233 ± 82	801 ± 5	434 ± 113	353 ± 152
PP/EVOH/PP	404 ± 4	282 ± 56	229 ± 73	226 ± 85	789 ± 3	437 ± 136	354 ± 158
APET/PE	338 ± 4	245 ± 38	200 ± 46	197 ± 58	648 ± 8	353 ± 92	292 ± 104
APET/PE/EVOH/PE	369 ± 3	277 ± 48	213 ± 56	218 ± 66	-	-	-
PA/PE	166 ± 2	125 ± 27	102 ± 39	95 ± 43	293 ± 5	160 ± 66	140 ± 83
PE/PA/EVOH/PA/PE	164 ± 3	121 ± 26	93 ± 39	90 ± 39	291 ± 3	165 ± 64	133 ± 70
PS/EVOH/PE	413 ± 3	279 ± 55	236 ± 62	223 ± 73	817 ± 3	430 ± 124	347 ± 73

Average thickness based on the measurement of ^a $n = 10$, ^b $n = 197$, ^c $n = 236$, ^d $n = 472$, and ^e $n = 287$ locations in ^a sheet or ^{b–e} tray samples.

Figure 2. Visual representation of percentage thinning in 25-, 50/R5-, 50-, and 75-trays of the thin (**left**) and thicker (**right**) PP sheets.

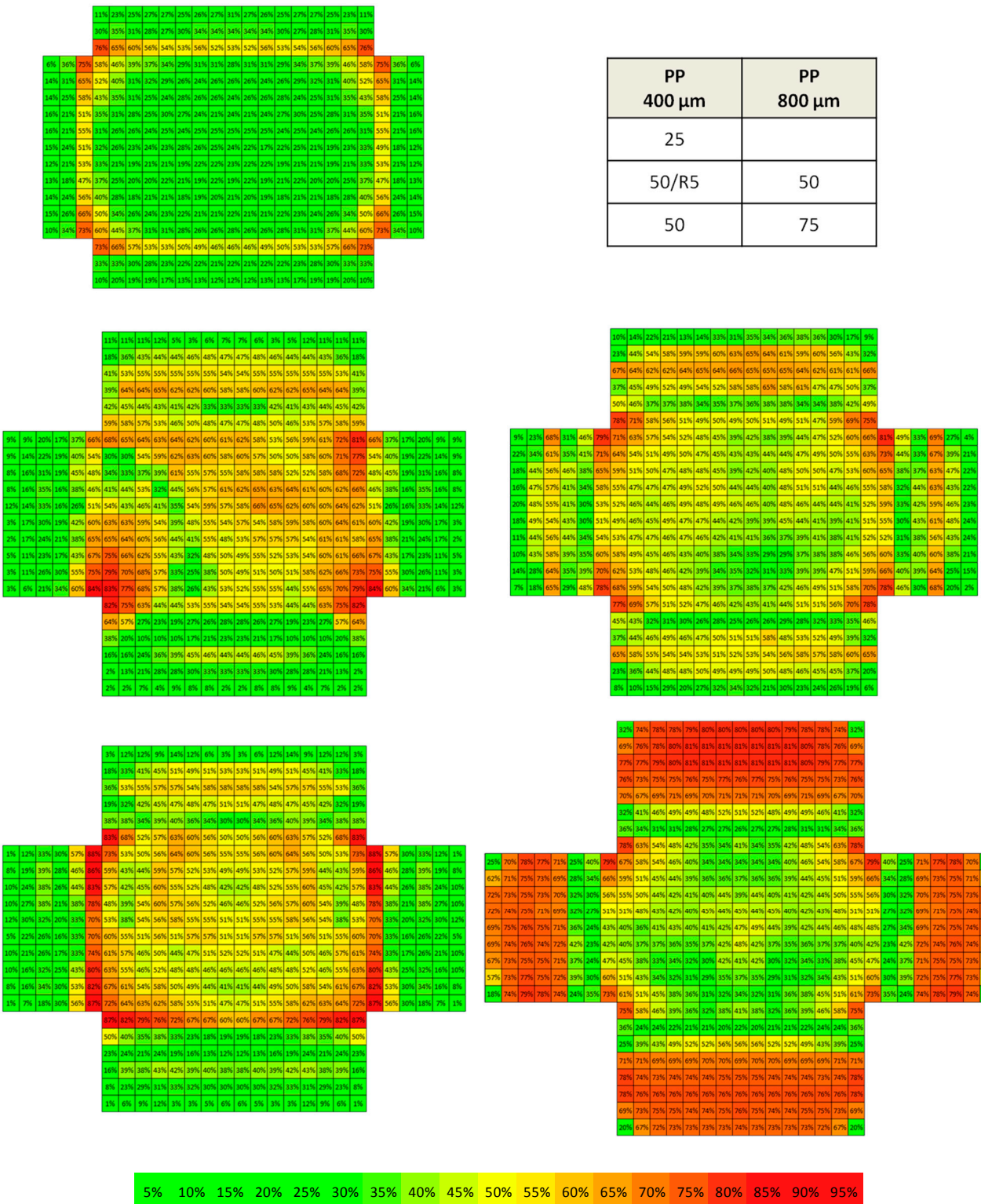


Figure 3. Visual representation of percentage thinning in 25-, 50/R5-, 50-, and 75-trays of the thin (**left**) and thicker (**right**) APET/PE sheets.

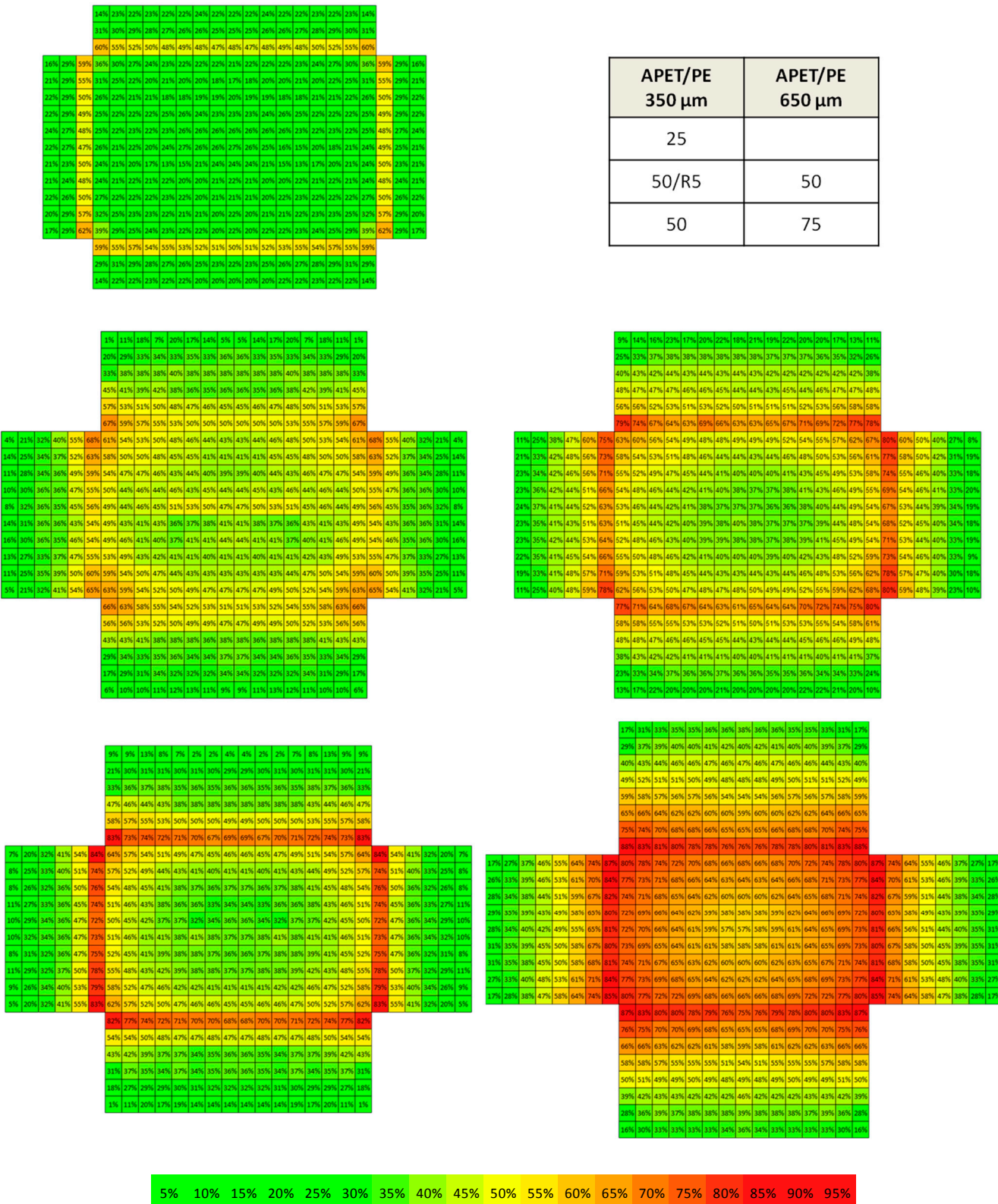


Figure 4. Visual representation of percentage thinning in 25-, 50/R5-, 50-, and 75-trays of the thin (**left**) and thicker (**right**) PA/PE sheets.

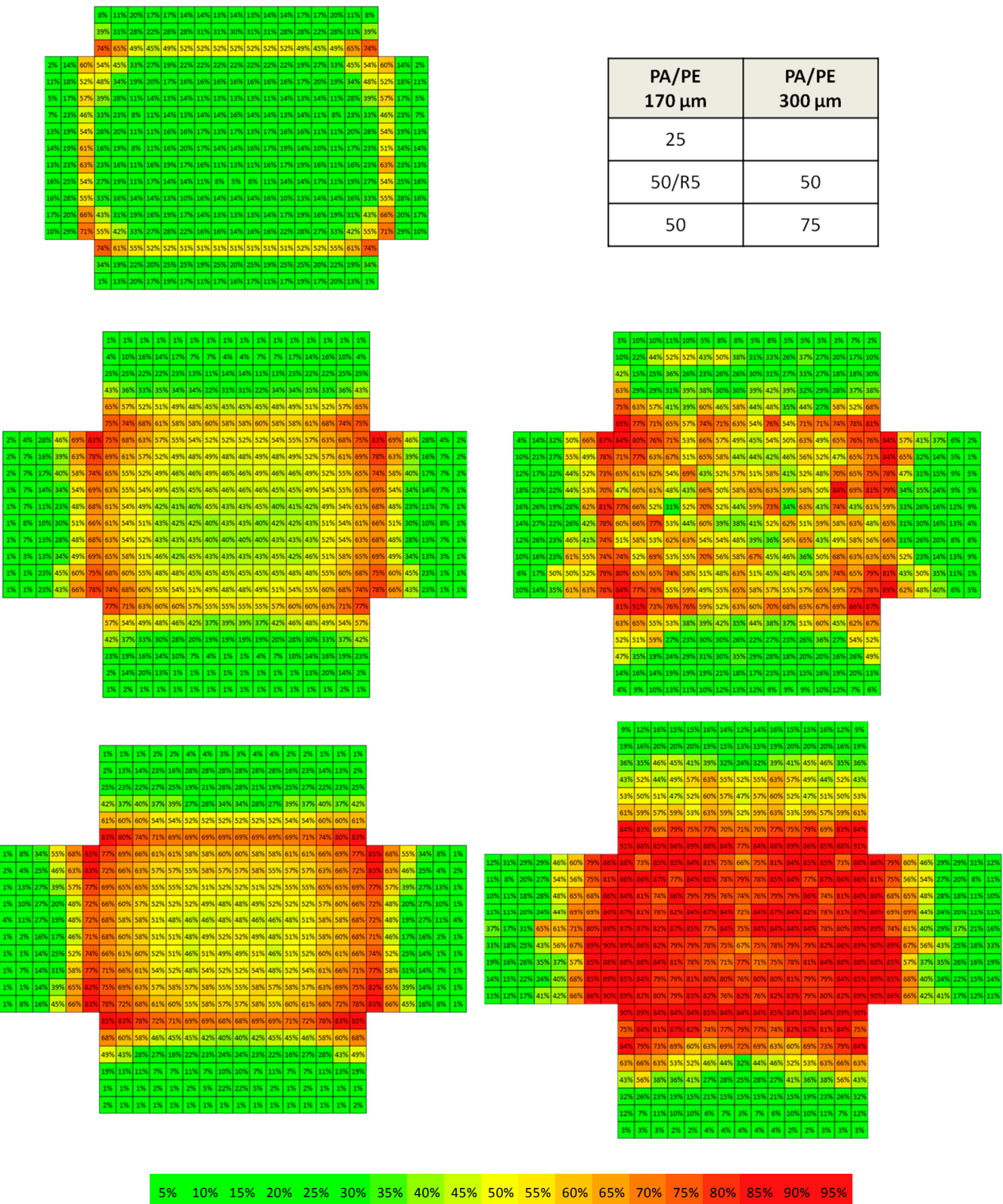
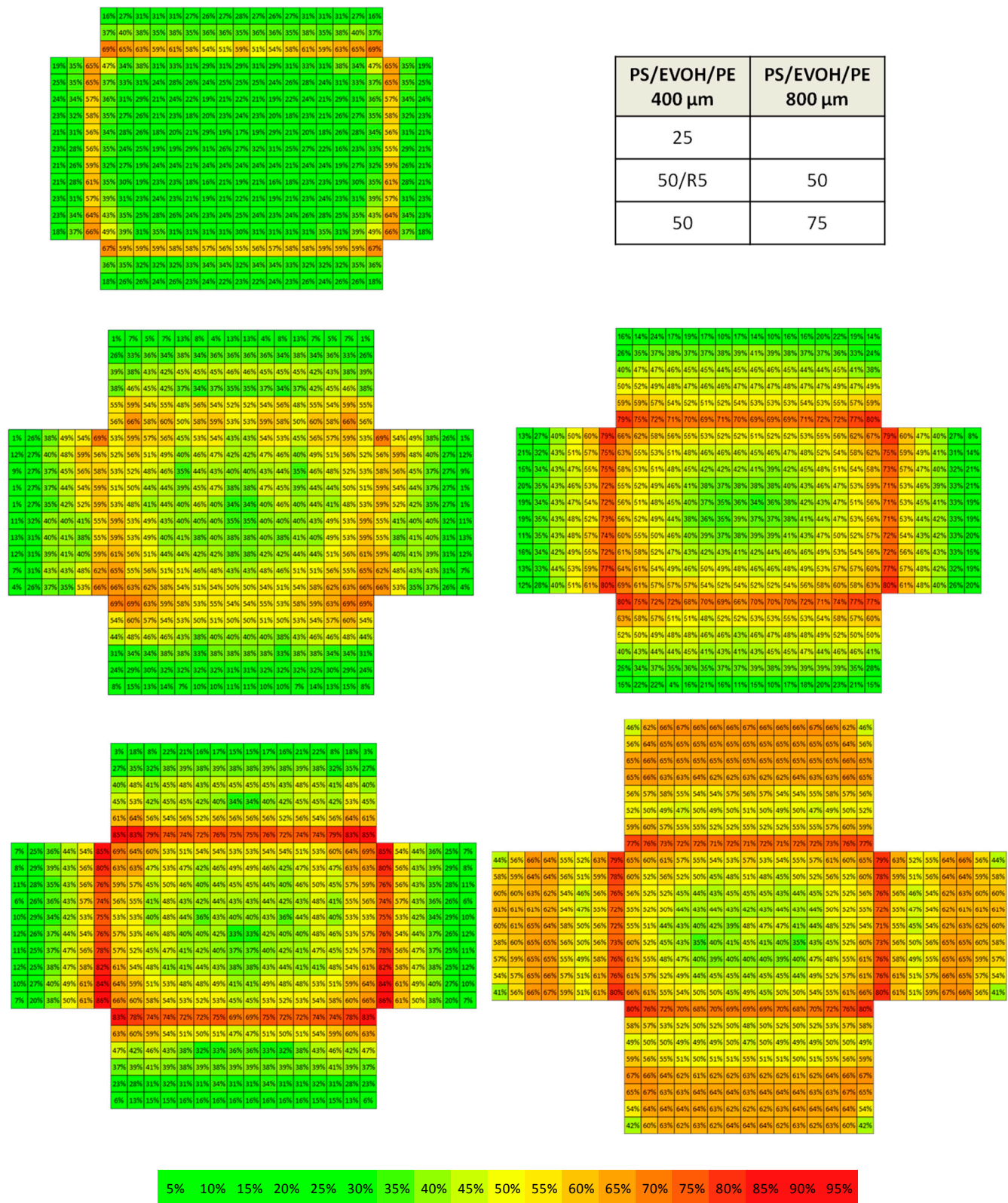


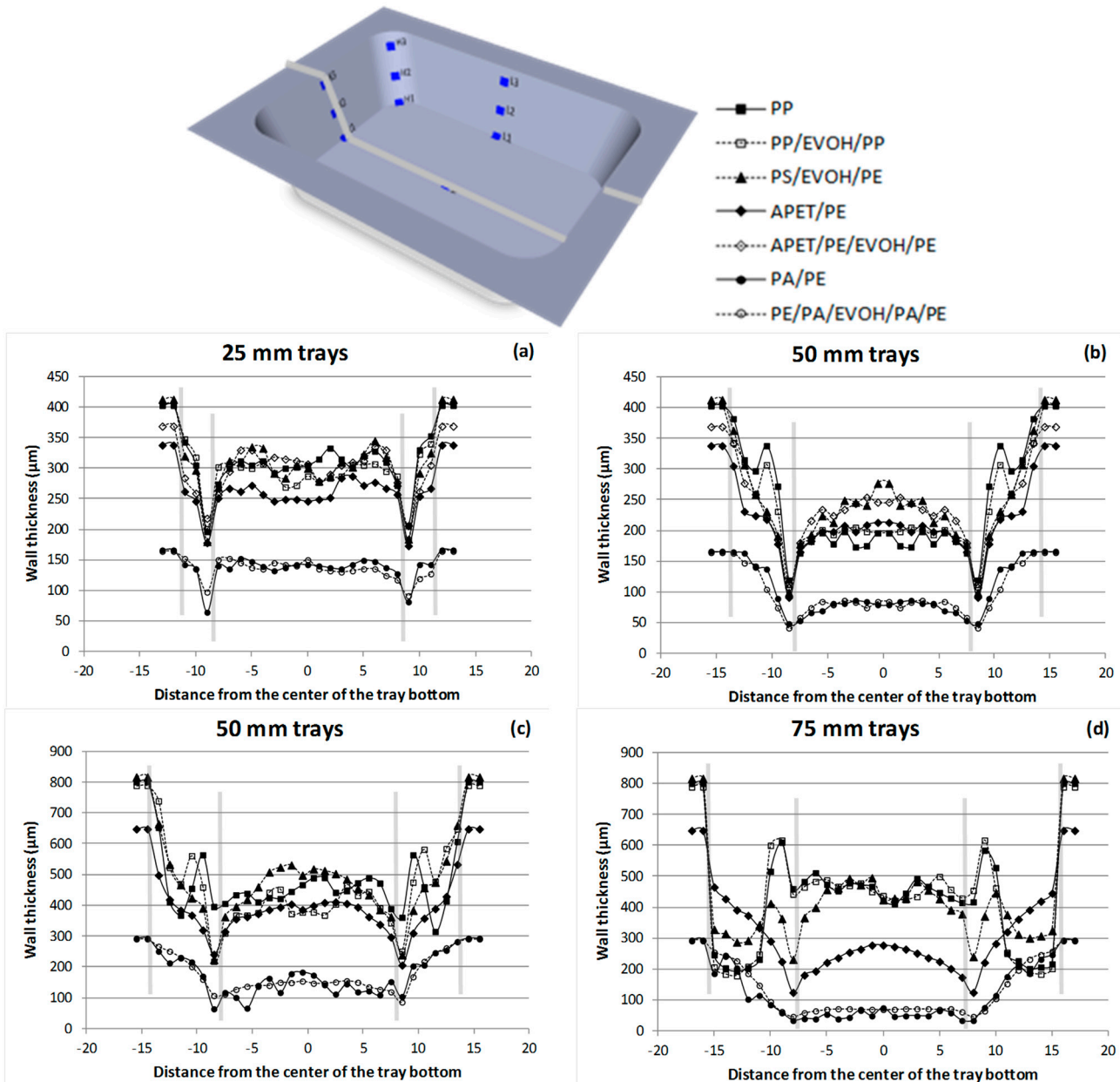
Figure 5. Visual representation of percentage thinning in 25-, 50/R5-, 50-, and 75-trays of the thin (**left**) and thicker (**right**) PS/EVOH/PE sheets.



To give a better insight into the absolute wall thickness of the formed trays, the measured wall thickness distribution was also plotted as a profile from the left piece of unconverted sheet over the middle of the short sidewall, through the center of the bottom, over the other short sidewall to the right

piece of unconverted sheet of the 25- and 50-mm trays of the thin sheet materials (Figure 6a,b) and the 50- and 75-mm trays of the thicker sheet materials (Figure 6c,d), respectively. Again, the profiles of the thin sheet materials clearly show that the edges are more thinned than the walls and the bottom. In addition, in the case of the 50-mm APET/PE trays, no difference in wall thickness distribution was observed after thermoforming trays with or without the aid of the plug (data not shown). The thicker sheet materials show more variation in wall thickness distribution, which might be related to the material characteristics and the parameters that were selected for the plug-assisted thermoforming process. In the case of the PP materials, the plug was optimized with rounded corners to obtain high-quality trays. For the PA materials, no plug was used, since this is generally not done in industrial processes. These results can add to further optimization of the thermoforming process.

Figure 6. Wall thickness distribution (μm) along a cross-section through the short side walls of the 25-mm (a) and 50-mm (b) trays and the thicker 50-mm (c) and 75-mm (d) trays. Distance from the center of the tray bottom is expressed in centimeter.



3.3. Oxygen Transmission Rate of Sheets versus Trays

In order to investigate how the material distribution before and after thermoforming relates to the oxygen barrier properties, the OTR of all sheets and trays was measured under the same conditions. In this study 50% RH outside and 90% RH inside the tray was chosen because of the relevance for a lot of potential food products. All tests were performed at standard lab conditions (23 °C). It should be remarked that a lot of food products are stored at 4 °C. Since the permeation and diffusion process is strongly temperature controlled, an Arrhenius model should be applied, from which the OTR can be extrapolated to other temperatures [23].

Since the OTR of sheets and trays was measured at oxygen pressure gradients of 0%–99.9% and 0%–20.9%, respectively, OTR values are expressed in [cc/m²·day·atm] for the sheets and in [cc/package·day·0.209·atm] for the trays. The latter were recalculated into [cc/package·day·atm]. In order to compare the OTR of sheets *versus* formed trays, the data were recalculated into the same units, by dividing the OTR of the tray by its surface area. Surface areas of trays with a depth of 25, 50, and 75 mm were respectively, 0.0361, 0.0471, and 0.0574 m². The exact surface area of the sheet (A_0) that is thermoformed into a tray was 0.0247 m².

3.3.1. Measured OTR

Table 4 shows the OTR of all tested materials. The PP sheets showed the lowest oxygen barrier properties (149.2 and 65.70 cc/m²·day·atm); the OTR of the APET/PE and PA/PE sheets ranged between 14.3 and 4.70 cc/m²·day·atm, depending on the respective sheet thickness; and the OTR of the multilayer sheets containing EVOH ranged from 0.48 to 1.7 cc/m²·day·atm. These results are in accordance with permeability data found in the literature, summarized by Vandewijngaarden *et al.* [24]. Furthermore, all EVOH-containing sheets showed OTR values below 2 cc/m²·day·atm, the limit value required for packaging applications of shelf-stable food [20]. The higher OTR of the PE/PA/EVOH/PA/PE multilayer can be explained by the EVOH type containing 38 mol% ethylene, exhibiting poorer barrier properties as compared to the 32 mol% ethylene types [19,25].

Table 4. Mean OTR ± standard deviation ($n = 2$ –3) of tested sheets and trays, expressed in cc/m²·day·atm.

Test materials	d_0	OTR _{sheet}	OTR ₂₅	OTR _{50/R5}	OTR ₅₀	OTR ₇₅
PP	403 µm	149.2 ± 0.5	179 ± 10	197 ± 3	234 ± 10	-
PP	801 µm	65.70 ± 0.05	-	88 ± 2	90 ± 2	129 ± 5
APET/PE	338 µm	10.1 ± 0.6	14 ± 2	18.5 ± 0.1	21 ± 2	-
APET/PE	648 µm	4.70 ± 0.04	-	-	9.3 ± 0.2	13.6 ± 0.3
PA/PE	166 µm	14.3 ± 0.3	20.95 ± 0.08	-	26.47 ± 0.05	-
PA/PE	293 µm	8.2 ± 0.7	-	-	21.3 ± 0.6	29.5 ± 0.3
PP/EVOH/PP	404 µm	0.93 ± 0.01	1.87 ± 0.02	3.42 ± 0.04	3.2 ± 0.2	-
PP/EVOH/PP	789 µm	0.52 ± 0.05	-	-	1.4 ± 0.2	2.32 ± 0.08
APET/PE/EVOH/PE	369 µm	1.5 ± 0.2	2.4 ± 0.5	-	2.5 ± 0.1	-
PS/EVOH/PE	413 µm	0.9 ± 0.2	1.5 ± 0.2	-	2.0 ± 0.2	-
PS/EVOH/PE	817 µm	0.48 ± 0.03	-	-	1.22 ± 0.02	1.18 ± 0.09
PA/EVOH/PA/PE	164 µm	0.69 ± 0.01	1.16 ± 0.02	-	1.22 ± 0.03	-
PE/PA/EVOH/PA/PE	291 µm	1.7 ± 0.1	-	-	2.8 ± 0.1	3.57 ± 0.07

The OTR results of the EVOH multilayer sheets with PP, PS, and APET were proportional to the thickness of the respective EVOH layers (Table 1). However, since EVOH resins are hygroscopic and readily absorb moisture depending on the ambient temperature and relative humidity, the oxygen barrier properties of EVOH are adversely affected by the amount of moisture absorbed [20]. This might explain the small variation observed with the PA/EVOH/PA/PE sheet containing only 8 μm EVOH and performing better than slightly thicker EVOH layers. In a study of Kuraray, the humidity and OTR of middle layer EVOH (EVALTM) in various sandwich structures was determined. These results indicate that the barrier properties of EVALTM resin layers can be optimized if a film with high moisture transmission rate such as PA is employed on the outside (65% RH) and LDPE on the inside when packaging high-moisture products (100% RH). According to this study, gas barrier properties are better as compared to low moisture transmission rate materials such as PP on the outside in analogous conditions [25]. Furthermore, care must be taken to determine the OTR, since it can take a long time before the EVOH-containing multilayer reaches equilibrium, especially when sandwiched between two low moisture transmission rate materials. In this respect, the measured OTR of the PP/EVOH/PP sheet at RH of 50% inside and 90% outside of the film could be a slight overestimation of the actual barrier properties [25].

In Table 4 and Figure 7, the OTR is shown as a function of the drawing depth for each material. The OTR at drawing depth 0 mm corresponds to OTR_{sheet}. In all cases the OTR of the trays increased with enhanced deep drawn depth. From these figures, one can clearly see the impact of using a thinner or thicker sheet material on the OTR of the tray, which can be of major importance from an economical and environmental point of view.

3.3.2. Theoretical OTR

It would also be interesting to predict the OTR of the trays based on the thickness and OTR of the sheet. This kind of calculation can be done based on the fact that the OTR is proportional to the area and inversely proportional to the thickness. The OTR of the tray was calculated according to Equation (2), with OTR₀ and d_0 the measured OTR in [$\text{cc}/\text{m}^2 \cdot \text{day} \cdot \text{atm}$] and thickness of the unconverted sheet, respectively; and A_i and d_i , the partial tray area and corresponding measured thickness, which are summed over the overall tray:

$$\text{OTR}_{\text{tray}} = \sum_{i=1}^n A_i \cdot \frac{d_0}{d_i} \cdot \text{OTR}_0 \quad (2)$$

The calculated OTR of the tray, OTR_{tray}, is then expressed in [$\text{cc}/\text{package} \cdot \text{day} \cdot \text{atm}$]. Under the assumption of a constant volume of the sheet during thermoforming, one could calculate the theoretical thickness of the tray according to Equation (3), with A_0 the area of the unconverted sheet; A_{tray} , the area of the tray; and d_{tray} the theoretical thickness of the tray:

$$A_0 \cdot d_0 = A_{\text{tray}} \cdot d_{\text{tray}} \quad (3)$$

The theoretical OTR of the trays can thus be calculated according to Equation (2), with $n = 1$; A_i the area of the tray, A_{tray} ; and d_i the theoretical thickness, d_{tray} , according to Equation (3) [5].

$$\text{OTR}_{\text{tray}} = A_{\text{tray}} \cdot \frac{d_0}{d_{\text{tray}}} \cdot \text{OTR}_0 = A_{\text{tray}} \cdot \frac{A_{\text{tray}}}{A_0} \cdot \text{OTR}_0 \text{ in } [\text{cc}/\text{package} \cdot \text{day} \cdot \text{atm}] \quad (4)$$

$$\frac{\text{OTR}_{\text{tray}}}{A_{\text{tray}}} = \frac{A_{\text{tray}}}{A_0} \cdot \text{OTR}_0 \text{ in } [\text{cc}/\text{m}^2 \cdot \text{day} \cdot \text{atm}] \quad (5)$$

Equation (5) was used to predict the normalized OTR values of the 25-mm, 50-mm, and 75-mm trays in Figure 7. These results are shown by the thin and thicker dashed lines for the respective sheet variants in all the graphs. Although this simplified calculation only considers the ratio of the sheet *versus* tray surface area, it seems to be quite a good approximation for materials, such as APET/PE (Figure 7b) and most EVOH multilayers. However, deviations of the measured data (\circ and \square) from the dashed line can be caused by various factors, such as uneven thinning (as shown in Figures 2–5), reorientation, or crystallization effects. In the case of monolayer PP, the measured OTR of the trays was far better than the predicted values (Figure 7a). In contrast, the predicted values of flexible PA/PE were rather an overestimate of the barrier properties as compared to the measured results (Figure 7c). In the case of the EVOH-containing multilayers, there was a variable deviation from the predicted values (Figure 7d–g).

Figure 7. Measured and theoretical OTR in $\text{cc}/\text{m}^2 \cdot \text{day} \cdot \text{atm}$ as function of the deep draw depth for (a) PP; (b) APET/PE; (c) PA/PE; (d) PP/EVOH/PP; (e) APET/PE/EVOH/PE; (f) PS/EVOH/PE; and (g) (PE)/PA/EVOH/PA/PE materials. Symbols \circ and \square represent the measured OTR of the thin and thicker sheet variant of each material, respectively. Dashed lines (···· and ---) represent the theoretical OTR based on Equation (5) for the thin and thicker sheet variants, respectively.

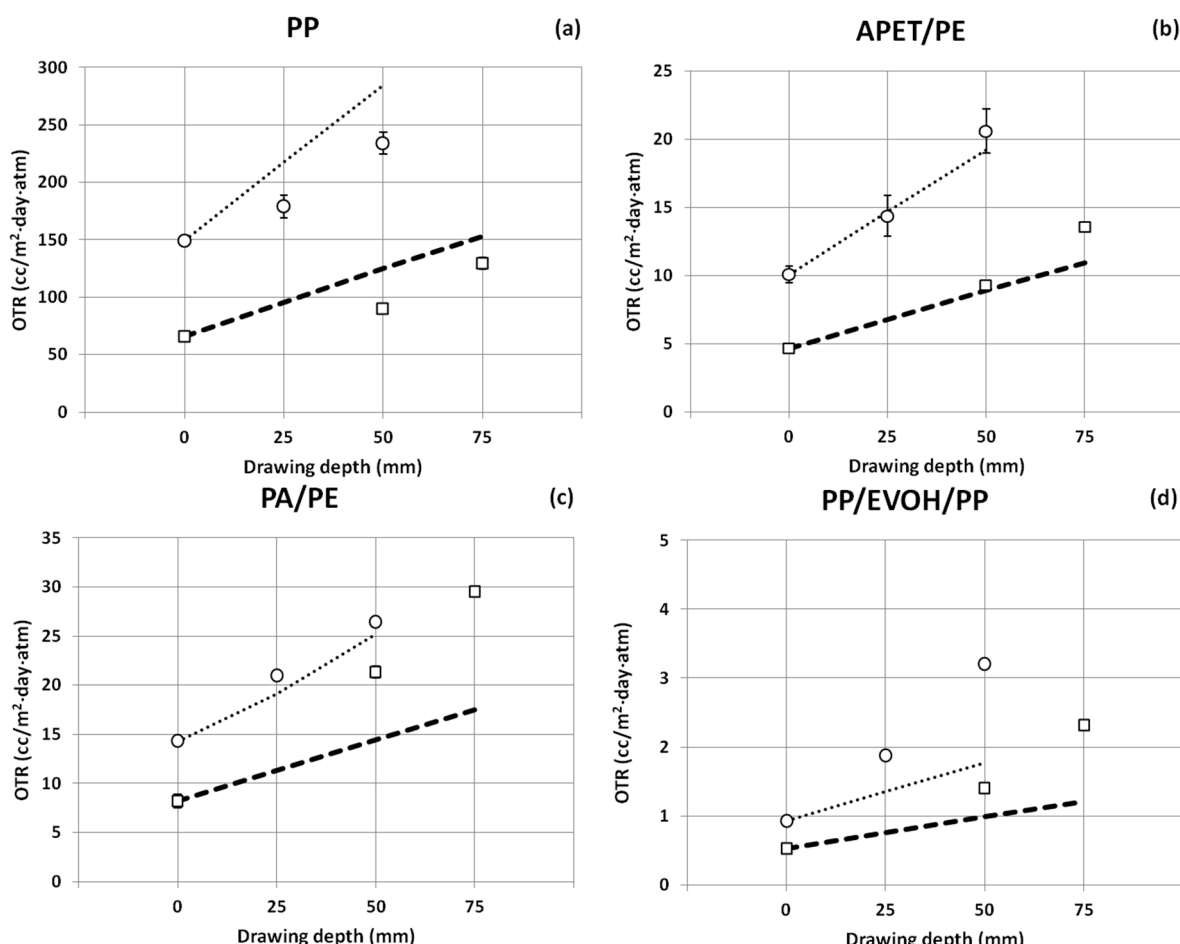
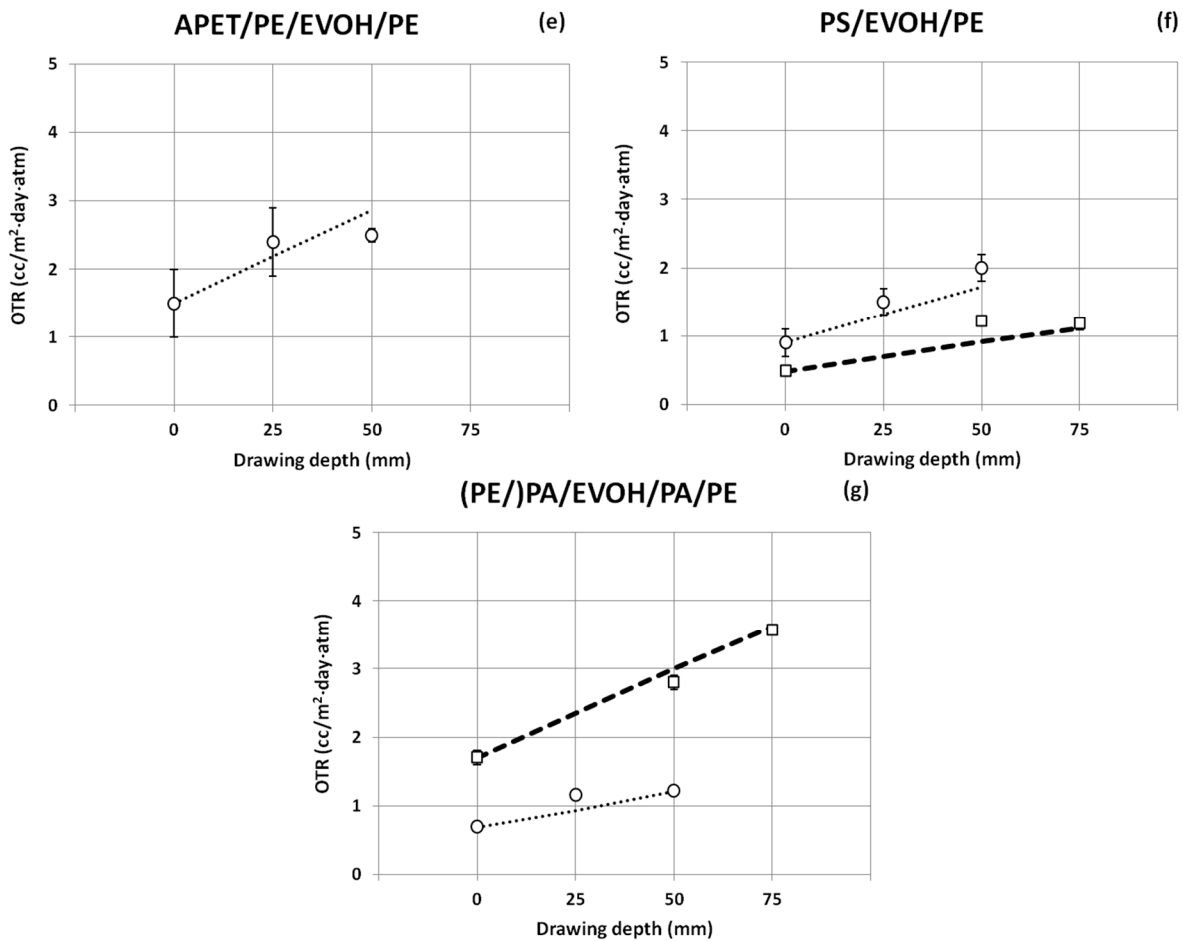


Figure 7. *Cont.*

3.4. Effect of (Re)Crystallization

The increase in OTR with increasing drawing depth is mainly the result of a reduction in material thickness. However, this negative effect can be countered by reorientation and (re)cristallization during thermoforming, which might improve the OTR [10]. The crystallinity of the polymer is a key parameter, since the permeant must seek out amorphous zones in order to penetrate a material. Therefore, a lower degree of crystallinity yields greater permeability. Increased molecular orientation reduces permeability, in effect making the path to permeate more difficult [26].

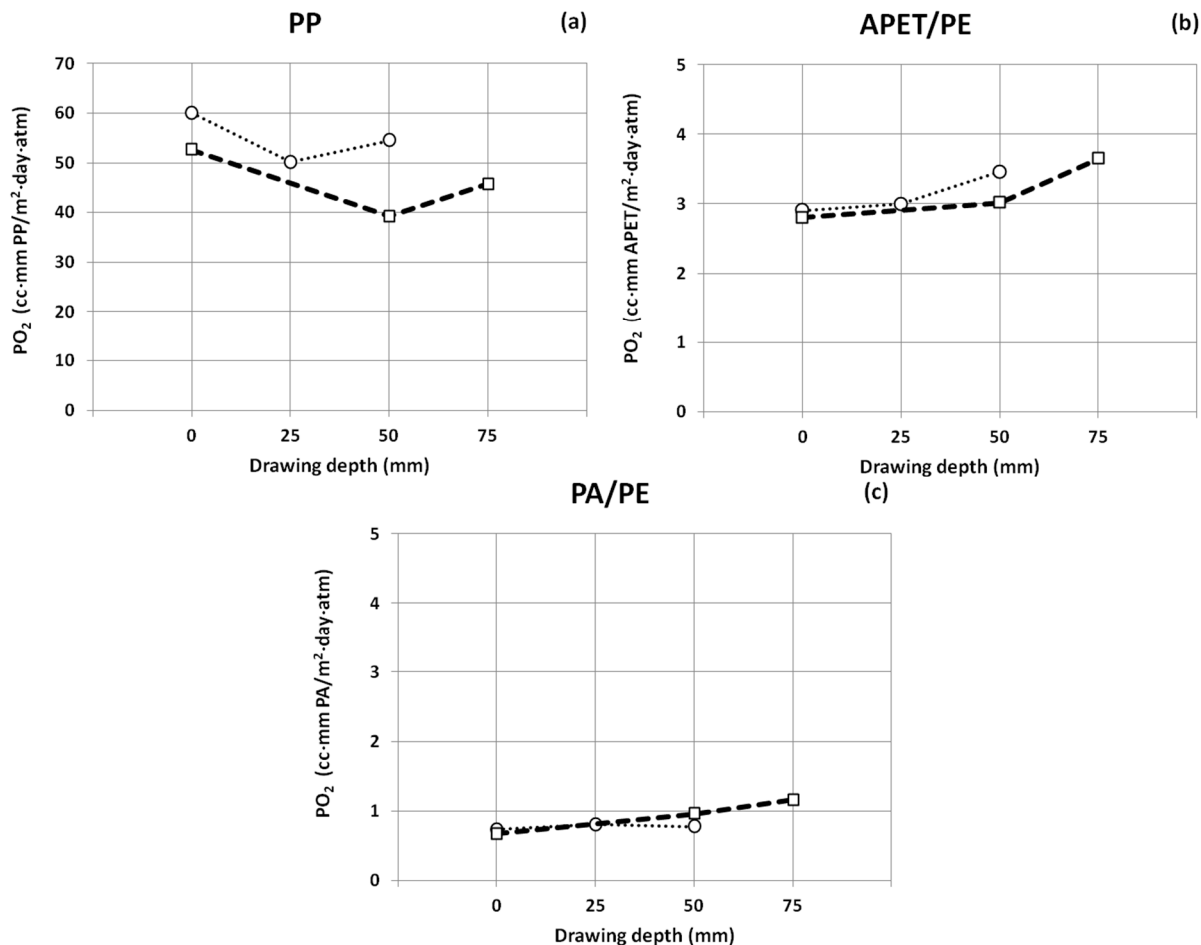
By normalizing the OTR data for relative sample thickness, the permeability coefficients (PO_2) expressed in $[\text{cc} \cdot \text{mm}/\text{m}^2 \cdot \text{day} \cdot \text{atm}]$ are useful to observe effects in addition to thinning or increase of the surface area. Equation (6) was applied, with n the number of layers; OTR the O_2 transmission rate of the multilayer in $\text{cc} \cdot \text{mm}/\text{m}^2 \cdot \text{day} \cdot \text{atm}$; d_i the thickness of i th layer in mm; and $PO_2(i)$ the permeability coefficient of i th layer in $\text{cc} \cdot \text{mm}/\text{m}^2 \cdot \text{day} \cdot \text{atm}$ [27]:

$$\frac{1}{OTR} = \sum_{i=1}^n \frac{d_i}{PO_2(i)} \quad (6)$$

In Figure 8, the PO_2 of the PP (a), APET (b), and PA (c) layers are shown as a function of the deep drawn depth. These values were calculated from the OTR of the PP, APET/PE, and PA/PE sheets

and trays, and the average thickness of the PP, APET, and PA layers, respectively, assuming that the contribution of PE to the oxygen barrier is negligible as compared to APET and PA [24].

Figure 8. Permeability coefficients of PP (a), APET (b), and PA layers (c) in sheets and trays, expressed in $\text{cc} \cdot \text{mm}/\text{m}^2 \cdot \text{day} \cdot \text{atm}$ as a function of the deep drawn depth. Connected symbols \circ and \square represent the PO_2 of the thin and thicker sheet variant of each material, respectively.



In the case of PP, the permeability coefficients of the trays were lower as compared to the sheet material (Figure 8a). This implies that the barrier properties had improved as a consequence of the thermoforming process. DSC analyses were performed on samples from the thin PP sheet and its 50-mm tray to explain the OTR results. The melt enthalpy (ΔH_m) of PP was significantly increased in three locations of the tray ($97 \pm 4 \text{ J/g}$ in a 3D corner; $101 \pm 2 \text{ J/g}$ in a 2D corner; and $101 \pm 4 \text{ J/g}$ in a side wall) as compared to the sheet material ($85 \pm 1 \text{ J/g}$; $p < 0.01$). The degree of crystallinity of PP (X_c) was increased from $41.3\% \pm 0.6\%$ in the unconverted sheet, to $47\% \pm 2\%$, $49\% \pm 1\%$, and $49\% \pm 2\%$ in the respective corners and wall of the tray. These results might explain why the measured OTR values in Figure 7a were better than the predicted values, since the latter only take into account material thinning. Obviously, the impact of the material thinning during thermoforming is anticipated by orientation and (re)crystallization of the PP chains, resulting in a better oxygen barrier than might be expected from the simplified theoretical thickness model [10].

APET's PO_2 was unchanged for the 25-mm and 50-mm trays, as compared to the thin and thick sheets, respectively. However, thermoforming to a deeper extent negatively affected APET's PO_2 in both the

thin and thicker material variants (Figure 8b). A DSC analysis was run on the 50-mm thin tray to measure the polymer's crystallinity. The ΔH_m of APET was only slightly increased in a 3D corner (40 ± 1 J/g) as compared to the sheet (36 ± 1 J/g) ($p < 0.05$), and no significant differences were observed in the 2D corner or wall. Based on the OTR results in Figure 7b, no positive effect of crystallization was expected; APET's X_c was $25.7\% \pm 0.8\%$ in the unconverted sheet *versus* $28.5\% \pm 0.9\%$ in the 3D corner, $26\% \pm 3\%$ in a 2D corner, and $27\% \pm 1\%$ in a thinned wall of the tray.

In the case of the thin PA/PE variant, PO_2 remained rather equal (Figure 8c). The DSC analysis showed an increased ΔH_m of PA in a 3D corner (26.9 ± 3.5 J/g, $p < 0.05$) and a 2D corner (25.0 ± 3.8 J/g, $p > 0.05$) of the 50-mm tray as compared to the ΔH_m of the sheet (19.0 ± 2.3 J/g). PA's X_c was slightly increased from $8\% \pm 1\%$ in the sheet to $12\% \pm 2\%$ and $11\% \pm 2\%$ in a 3D and 2D corner, respectively. In contrast, the barrier properties of the thick PA/PE variant got worse during thermoforming (Figure 8c). No significant effects were observed on the ΔH_m of PA in either a 3D corner (18.6 ± 1.2 J/g) or a 2D corner (18.8 ± 0.1 J/g) of the 50-mm tray, as compared to the ΔH_m of the sheet (18.9 ± 0.3 J/g). Deviation from the theoretical OTR values might be further explained by unequal thinning (Figure 4) and shrinkage after thermoforming.

3.5. EVOH Multilayer Materials

It is more difficult to explain the observed differences between the measured and predicted OTR values of the EVOH-containing multilayers in Figure 7. The EVOH gas barrier properties are dependent on various factors, such as the thickness of the EVOH layer, which varies throughout the tray, but also on the RH inside and outside the package, and the thickness and water vapor transmission rate of the constituent layers [19,28,29]. Furthermore, EVOH copolymers are semi-crystalline and the crystallinity, orientation, chain stiffness, free volume, and cohesive energy density of the polymer influence the barrier properties as well [28,30]. The crystallinity of EVOH might be affected by parameters of the thermoforming process, e.g., the thermoforming temperatures of the respective multilayers are different, as shown in Table 2. The effect on gain or loss of crystallinity of EVOH requires further in-depth study by other techniques, as the melt enthalpy of this polymer was too small to obtain accurate results from the DSC profiles.

In addition, all samples were measured at a RH of 50% outside and 90% inside the trays. It is known that water molecules absorbed by EVOH at a high RH can interact with the hydroxyl groups in the EVOH matrix and weaken the hydrogen bonds between the polymer molecules. This plasticizing effect can impair the barrier properties of hydrophilic polymers [19]. Therefore, the barrier properties of the PP/EVOH/PP, APET/PE/EVOH/PE, PS/EVOH/PE, and (PE/)PA/EVOH/PA/PE multilayers are also dependent on the thickness and water vapor transmission rate of the sandwich layers [19,29]. The presence of small molecules such as water in the polymer matrix may change the way oxygen is sorbed and diffused in a polymer. Hernandez has discussed different interaction mechanisms of water and oxygen within PA polymers, including self-association of water molecules and oxygen/water molecular competition [31].

In order to acquire deeper insight into the OTR of the EVOH multilayers, microscopic thickness measurements of the individual layers were performed in strategic locations such as the long (L) and short (K) side wall, a 3D corner (H), and the bottom (B) of all tray types (Figure 9). The portion of

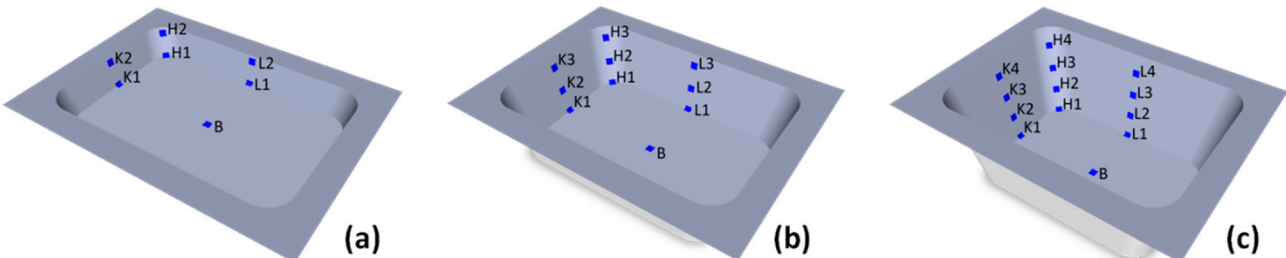
EVOH as compared to the actual total thickness in each location was expressed as percentage EVOH. The average EVOH% in the respective locations of three trays was compared to the initial EVOH% in the sheets. These results indicated that the EVOH layer, in general, was reduced proportionally with the global thickness (EVOH% remained about the same). Nonetheless, the EVOH layers in locations close to the bottom (L_1 , K_1 , and H_1) were the most reduced during thermoforming. Table 5 shows the minimum and maximum EVOH% that were measured in the respective locations shown in Figure 9.

Table 5. Minimum and maximum portion of EVOH in the layer distribution in locations K_i , L_i , H_i , and B_i of the trays as compared to the average EVOH% in the respective sheet materials.

Multilayer	sheet	tray ₂₅ ^a	tray ₅₀ ^b	sheet	tray ₅₀ ^b	tray ₇₅ ^c
PP/EVOH/PP	3.2%	1.5%–3.2%	1.8%–3.5%	3.0%	1.9%–3.7%	2.0%–4.4%
PS/EVOH/PE	2.9%	1.9%–3.5%	2.1%–3.4%	3.1%	1.8%–3.3%	1.8%–3.5%
APET/PE/EVOH/PE	2.7%	1.8%–4.1%	1.5%–3.0%	-	-	-
PE/PA/EVOH/PA/PE	4.9%	3.8%–5.6%	3.6%–5.4%	4.1%	3.4%–4.9%	3.1%–4.3%

Min%–max% EVOH measured in locations shown in Figure 9a ^a, b ^b and c ^c ($n = 3$ trays).

Figure 9. Locations in 25- (a), 50- (b), and 75-mm (c) trays that were analyzed microscopically for individual layer thickness. Locations L, K, H, and B were selected in the long side wall, short side wall, corner, and bottom, respectively.



In addition, the absolute values of the average EVOH layer thickness in the most critical locations are shown in Table 6. In this study, the minimum thickness of the EVOH layer was $1.5 \mu\text{m} \pm 0.2 \mu\text{m}$ (H_1); $1.4 \mu\text{m} \pm 0.3 \mu\text{m}$ (H_1); $2.5 \mu\text{m} \pm 0.3 \mu\text{m}$ (K_1); and $1.1 \pm 0.1 \mu\text{m}$ (H_1) in the 50-mm trays of the thin variants of PP/EVOH/PP; APET/PE/EVOH/PE; PS/EVOH/PE; and PA/EVOH/PA/PE, respectively.

In the thicker variants, EVOH was also most reduced in locations L_1 , K_1 , and H_1 (Table 6), except for the 75-mm PP/EVOH/PP tray, where locations L_3 , K_3 , H_1 , and H_3 ($5.7 \pm 0.7 \mu\text{m}$, $6.5 \pm 1.2 \mu\text{m}$, $4.5 \pm 0.6 \mu\text{m}$, and $5.5 \pm 0.6 \mu\text{m}$, respectively) showed the thinnest EVOH layers, which could be expected from Figure 2. These results give a quantitative impression of the impact of the thermoforming process on the EVOH layer thickness.

Table 6. EVOH layer thickness in the most critical locations of the tray *versus* sheet material in μm .

Multilayer	Tray type	Sheet ^a	L_1 ^b	K_1 ^b	H_1 ^b
PP/EVOH/PP	tray ₂₅	13 ± 1	3.2 ± 0.7	4.1 ± 0.6	2.7 ± 0.8
	tray ₅₀	13 ± 1	2.4 ± 0.2	2.4 ± 0.5	1.5 ± 0.2
PS/EVOH/PE	tray ₂₅	12 ± 2	3.5 ± 0.6	4.7 ± 0.3	3.8 ± 0.7
	tray ₅₀	12 ± 2	2.6 ± 0.3	2.5 ± 0.3	2.9 ± 0.5
APET/PE/EVOH/PE	tray ₂₅	10 ± 1	3.1 ± 0.5	4.4 ± 0.4	2.4 ± 0.7
	tray ₅₀	10 ± 1	2.2 ± 0.4	1.6 ± 0.2	1.4 ± 0.3
PA/EVOH/PA/PE	tray ₂₅	8 ± 1	3.0 ± 0.3	3.8 ± 0.5	2.8 ± 0.2
	tray ₅₀	8 ± 1	2.4 ± 0.2	2.3 ± 0.2	1.1 ± 0.1
PP/EVOH/PP	tray ₅₀	24 ± 2	8.8 ± 1.1	5.3 ± 1.5	3.3 ± 0.4
	tray ₇₅	24 ± 2	10.5 ± 1.4	11.5 ± 2.1	4.5 ± 0.6
	tray ₇₅	24 ± 2	5.7 ± 0.7 (L_3)	6.5 ± 1.2 (K_3)	5.5 ± 0.6 (H_3)
PS/EVOH/PE	tray ₅₀	24 ± 3	5.0 ± 0.6	5.9 ± 2.1	3.3 ± 0.7
	tray ₇₅	24 ± 3	4.9 ± 1.1	5.8 ± 0.7	3.9 ± 0.1
PE/PA/EVOH/PA/PE	tray ₅₀	12 ± 1	4.8 ± 0.3	3.9 ± 0.7	2.6 ± 0.6
	tray ₇₅	12 ± 1	2.2 ± 0.2	1.9 ± 0.2	1.3 ± 0.2

^a $n = 10$; ^b $n = 3$.

In summary, the presence of an EVOH layer (~3%) in the PP variants resulted in OTR values that were 160, 96, and 73 times better than the OTR values of the thin PP monolayer sheet and the 25- and 50-mm trays, respectively. In the case of the thicker PP variants, the OTR values of the PP/EVOH/PP sheet, 50-, and 75-mm trays were improved with a factor of 126, 64, and 56, respectively, as compared to the monolayer PP samples. As discussed in Section 3.3.1, the measured oxygen barrier of the PP/EVOH/PP sheets might be an overestimation. In addition, the OTR of the PA/EVOH/PA/PE sheet and the 25- and 50-mm trays (~4.9% EVOH) was 21, 18, and 22 times better than the respective sheet and trays without an EVOH layer, and the OTR of the APET/PE/EVOH/PE sheet and 25- and 50-mm trays (2.7% EVOH) was 7, 6, and 8 times better than the respective sheet and trays without an EVOH layer. Furthermore, the importance of considering the mol% ethylene in the EVOH grade was shown in the OTR of the PE/PA/EVOH/PA/PE sheet and the 50- and 75-mm trays (4.1% of 38 mol% ethylene EVOH), which were improved by a factor of only 5, 8, and 8 as compared to the samples without EVOH.

3.6. Impact of Tray Design on the OTR

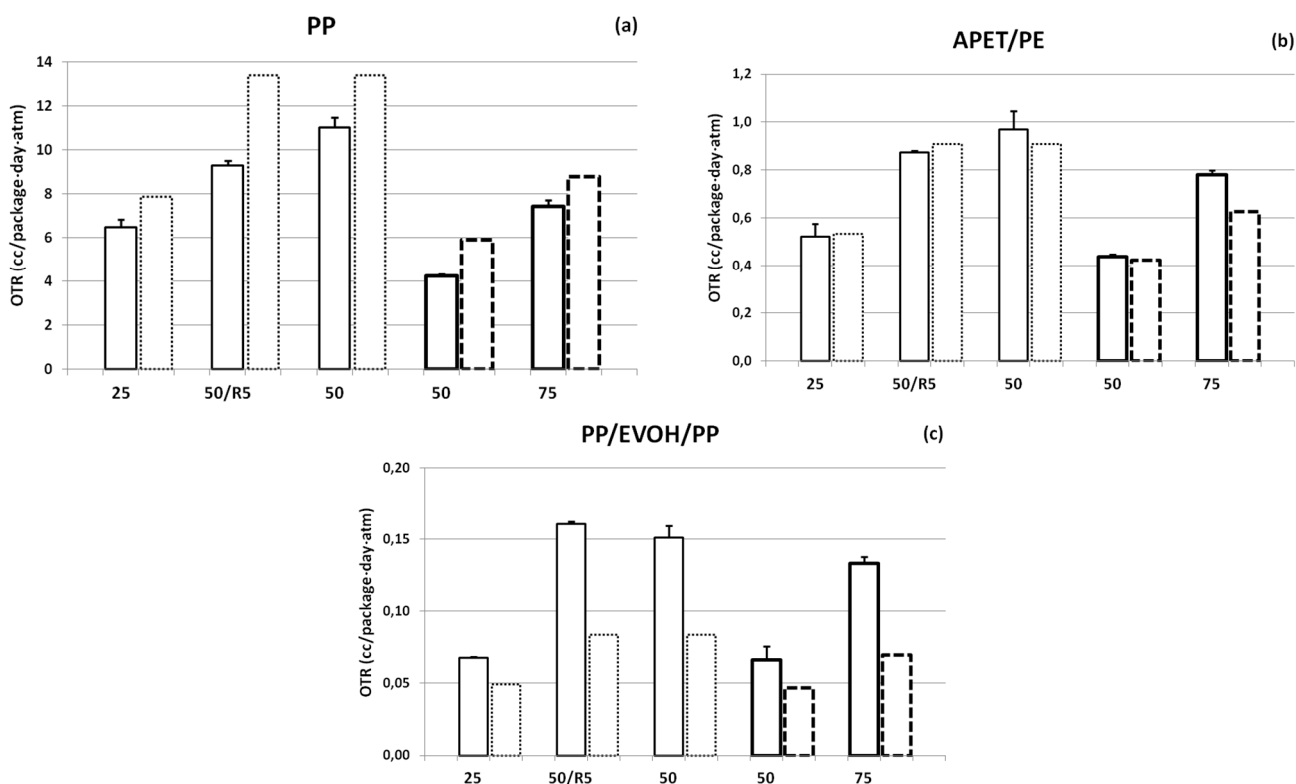
So far, the effect of increased exposed area of the thermoformed trays is eliminated from the previous expressions of the OTR data. With regard to the application of a tray as a food packaging, it is important to consider the exposed area and express the OTR of the trays in [cc/package·day·atm].

Figure 10 shows the OTR data of the 25-, 50-/R5, 50-, and 75-mm trays of PP, APET/PE, and PP/EVOH/PP expressed in [cc/package·day·atm]. These figures clearly demonstrate the impact of the thickness of the sheet material, as well as the impact of the deep drawing depth and the effect of round corners, on the final OTR of the thermoformed trays. The uneven thinning of PP (shown in Figure 2), which was increasingly observed in the 25-, 50/R5- and 50-mm trays, clearly corresponds to an enhanced OTR – from 6.5 ± 0.4 to 9.3 ± 0.2 and 11.0 ± 0.5 cc/package·day·atm in the respective trays

(Figure 10a). The same phenomenon was observed for the APET/PE materials, showing OTR values of 0.5 ± 0.1 , 0.87 ± 0.01 , and 1.0 ± 0.1 cc/package·day·atm, respectively (Figure 10b). These results indicate that modifying the mold design to form trays with round corners has a beneficial effect on the final OTR of the tray [32,33].

In contrast, no significant effect of round corners was observed for PP/EVOH/PP multilayers (Figure 10c). Furthermore, since the OTR of the 25- and 50-mm trays of APET/PE/EVOH/PE and PA/EVOH/PA/PE were in close proximity (Table 4), no significant effect was expected from a tray design with round corners either.

Figure 10. OTR results expressed in cc/package·day·atm. Bars in thin and thick lines represent the measured OTR of the trays from the thin and thicker (a) PP; (b) APET/PE; and (c) PP/EVOH/PP material variants, respectively; bars in thin and thicker dotted lines (···· and ---) represent the theoretical OTR based on Equation (4) for the thin and thicker sheet variants, respectively.



3.7. Simulation of the Oxygen Level in the Packaging

In practice it will be important to estimate the barrier properties in terms of the shelf life of a food product in specific storage conditions or the time when a specific percentage of oxygen will be present in the package at a specific storage temperature. The O₂ concentration in the packaging is determined by the residual O₂ after packaging, the respiration or consumption of O₂ by the product, and by the O₂ ingress during the shelf life (OTR) [34,35]. The simulation software PredOxyPack® is a practical tool to predict the oxygen ingress for different packaging configurations, materials, and time–temperature profiles [36]. In this way, realistic estimations can be made for the circumstances to which food is exposed during its preservation including cold chain conditions [37].

Using the OTR data obtained in this study combined with the following settings of simulation: (i) an impermeable seal film; (ii) tray filled with 50% headspace; (iii) a residual level of 0.5% O₂ after filling; and (iv) a time temperature profile of 20 months at 21 °C—the O₂ evolution in the package was calculated for the different EVOH-trays. After 20 months, the O₂ concentration under the simulation conditions would be 3.5% and 3.7% for the 50 and 50/R5 PP/EVOH/PP trays, respectively; and 2.9%, 2.3%, and 1.8% for the thin 50-mm APET/PE/EVOH/PE, PS/EVOH/PE, and PA/EVOH/PA/PE trays, respectively. In addition, the O₂ concentration under the same simulation conditions would be 3.7%, 3.0%, 2.5%, and 2.2% for the 25-mm APET/PE/EVOH/PE, PP/EVOH/PP, PS/EVOH/PE, and PA/EVOH/PA/PE trays, respectively.

4. Conclusions

In this study, the effect of variable drawing depths and radii of the corners on the thickness and final OTR of thermoformed trays of nine conventional semi-rigid and four flexible packaging materials was measured and analyzed. An overview of all results can be consulted via the interactive MaProDe_Ox tool (<http://www.uhasselt.be/VerpakingsCentrum>). The material thickness distribution in corners, walls, and bottom was dependent on the test material and its forming process. The OTR of the trays increased with the drawing depth, but this effect could be improved in the case of PP and APET/PE by increasing the radius of the corners. It would have been interesting to investigate these effects on trays with a 75 mm depth; however, these trays would probably not have met with commercial acceptance. The results show that the EVOH layers were sufficient for deep drawing to depths of 25, 50, and 75 mm for the selected multilayer materials and that the EVOH layers, in general, were thinned proportionally with global thickness.

This study further indicates that the predicted OTR, based on a homogeneous material distribution, can be used as a rough approximation of the real OTR. Since this simplified calculation only takes into account the ratio of the surface area of the sheet and the tray, detailed analysis of unequal thinning, orientation, and (re)crystallization remains necessary to explain the deviation (upwards or downwards) of the measured OTR as compared to the predicted one. Certainly in the case of monolayer PP, there is potential for improvement of the OTR as compared to the predicted value, due to reorientation of PP polymers during deep drawing.

Finally, the significance of the obtained OTR values requires translation in terms of the oxygen level in the package that will finally determine the shelf life of the product in a modified atmosphere packaging. The results from this study contribute substantially to the knowledge of oxygen ingress in thermoformed trays in external conditions of 50% *versus* 90% RH inside at 23 °C with respect to different common packaging materials, the sheet thickness, and the design of the tray. Further studies may elaborate on additional materials and/or the effect of other temperatures and % RH.

Supplementary Materials

Supplementary materials can be accessed at: <http://www.mdpi.com/2073-4360/6/12/3019/s1>.

Acknowledgments

The MaProDe_Ox project “Impact of Material, Process & Design on the Oxygen Permeability of Thermoformed Packaging” was supported by grants from Flanders’ Food (FF). The authors would like to thank all participating companies from the Belgian packaging and food industry and Pack4FOOD for their contribution and constructive cooperation. We especially thank Steven van Campenhout (FF) for administrative support, Benny De Groof and Jan Mortier for excellent assistance in thermoforming the samples at Cobelplast, Didier Houssier and Geert Herremans (Kuraray, EVAL Europe) for helpful discussions about the results, Martine Van Hamel (research group of Applied and Analytical Chemistry) for performing the DSC experiments, and An Vermeulen and Peter Ragaert (Pack4FOOD) for support using PredOxyPack®.

Author Contributions

All listed authors contributed to the concepts and interpretation of obtained data in this work and the final manuscript. This multidisciplinary research project was supervised and acquired by Mieke Buntinx in collaboration with Roos Peeters. Most of the reported research was performed by Gert Willems. OTR measurements and interpretation were done with the support of Dimitri Adons (Packaging Center). DSC analysis and DSC data treatment were executed within Applied and Analytical Chemistry research group (Robert Carleer and Jan Yperman). The manuscript was prepared by Mieke Buntinx.

Conflicts of Interest

The authors declare no conflict of interest.

References

1. Czerniawski, B. Analysis of plastics packaging domestic market. *Polimery* **2007**, *52*, 811–819.
2. Throne, J.L. *Understanding Thermoforming*; Carl Hanser Verlag: Munich, Germany, 2008.
3. Li, Z.Z.; Heo, K.S.; Xuan, D.J.; Seol, S.Y. A study on cooling efficiency using 1-d analysis code suitable for cooling system of thermoforming. *J. Mech. Sci. Technol.* **2009**, *23*, 607–613.
4. Pettersen, M.K.; Gallstedt, M.; Eie, T. Oxygen barrier properties of thermoformed trays manufactured with different drawing methods and drawing depths. *Packag. Technol. Sci.* **2004**, *17*, 43–52.
5. Pettersen, M.K.; Nilsson, A.; Espedal, A.; Kohler, A. Prediction of oxygen transmission rate for thermoformed trays. *Packag. Technol. Sci.* **2004**, *17*, 321–332.
6. Crippa, A.; Sydenstricker, T.H.D.; Amico, S.C. Evaluation of multilayer thermoformed films for food packaging. *Polym. Plastics Technol. Eng.* **2008**, *47*, 991–995.
7. Rosen, S.R. *Thermoforming: Improving Process Performance*; Society of Manufacturing Engineers: Dearborn, MI, USA, 2002; pp. 155–179.
8. Martin, P.J.; Duncan, P. The role of plug design in determining wall thickness distribution in thermoforming. *Polym. Eng. Sci.* **2007**, *47*, 804–813.

9. Erdogan, E.S.; Eksi, O. Prediction of wall thickness distribution in simple thermoforming moulds. *J. Mech. Eng.* **2014**, *60*, 195–202.
10. Makradi, A.; Ahzi, S.; Belouettar, S.; Ruch, D. Thermoforming process of semicrystalline polymeric sheets: Modeling and finite element simulations. *Polym. Sci. Ser. A* **2008**, *50*, 550–557.
11. Robertson, G.L. Orientation. In *Food Packaging: Principles and Practice*; CRC Press: London, UK, 2013; pp. 152–155.
12. Aroujalian, A.; Ngadi, M.O.; Emond, J.P. Wall thickness distribution in plug-assist vacuum formed strawberry containers. *Polym. Eng. Sci.* **1997**, *37*, 178–182.
13. Chen, S.C.; Huang, S.T.; Lin, M.C.; Chien, R.D. Study on the thermoforming of PC films used for in-mold decoration. *Int. Commun. Heat Mass Transf.* **2008**, *35*, 967–973.
14. O'Connor, C.P.J.; Martin, P.J.; Sweeney, J.; Menary, G.; Caton-Rose, P.; Spencer, P.E. Simulation of the plug-assisted thermoforming of polypropylene using a large strain thermally coupled constitutive model. *J. Mater. Process. Technol.* **2013**, *213*, 1588–1600.
15. Giménez, E.; Lagarón, J.M.; Cabedo, L.; Gavara, R.; Saura, J.J. Study of the thermoformability of ethylene-vinyl alcohol copolymer based barrier blends of interest in food packaging applications. *J. Appl. Polym. Sci.* **2004**, *91*, 3851–3855.
16. Mueller, K.; Schoenweitz, C.; Langowski, H.C. Thin laminate films for barrier packaging application-influence of down gauging and substrate surface properties on the permeation properties. *Packag. Technol. Sci.* **2012**, *25*, 137–148.
17. *Standard Test Method for Determination of Oxygen Gas Transmission Rate, Permeability and Permeance at Controlled Relative Humidity through Barrier Materials Using a Coulometric Detector*; ASTM F1927; ASTM International: West Conshohocken, PA, USA, 2007.
18. *Standard Test Method for Oxygen Transmission Rate through Dry Packages Using a Coulometric Sensor*; ASTM F1307; ASTM International: West Conshohocken, PA, USA, 2007.
19. Yamamoto, T.; Kanda, T.; Nishihara, Y.; Ooshima, T.; Saito, Y. Correlation study among oxygen permeability, molecular mobility, and amorphous structure change of poly(ethylene-vinylalcohol copolymers) by moisture. *J. Polym. Sci. B Polym. Phys.* **2009**, *47*, 1181–1191.
20. Mokwena, K.K.; Tang, J. Ethylene vinyl alcohol: A review of barrier properties for packaging shelf stable foods. *Crit. Rev. Food Sci. Nutr.* **2012**, *52*, 640–650.
21. Ayhan, Z.; Zhang, Q.H. Wall thickness distribution in thermoformed food containers produced by a Benco aseptic packaging machine. *Polym. Eng. Sci.* **2000**, *40*, 1–10.
22. Collins, P.; Harkin-Jones, E.M.A.; Martin, P.J. The role of tool/sheet contact in plug-assisted thermoforming. *Int. Polym. Process.* **2002**, *17*, 361–369.
23. Vieth, W.R. *Diffusion in and through Polymers: Principles and Applications*; Hanser Publishers: Munich, Germany, 1991.
24. Vandewijngaarden, J.; Murariu, M.; Dubois, P.; Carleer, R.; Yperman, J.; Adriaensens, P.; Schreurs, S.; Lepot, N.; Peeters, R.; Buntinx, M. Gas permeability properties of poly(3-hydroxybutyrate-co-3-hydroxyhexanoate). *J. Polym. Environ.* **2014**, *22*, 1–7.
25. Kuraray. EVAL™ EVOH Resins. Available online: http://www.eval.eu/media/15492/technical%20brochure_english.pdf (accessed on 1 September 2014).
26. Hiltner, A.; Liu, R.Y.F.; Hu, Y.S.; Baer, E. Oxygen transport as a solid-state structure probe for polymeric materials: A review. *J. Polym. Sci. B Polym. Phys.* **2005**, *43*, 1047–1063.

27. Mastromatteo, M.; Del Nobile, M.A. A simple model to predict the oxygen transport properties of multilayer films. *J. Food Eng.* **2011**, *102*, 170–176.
28. Zhang, Z.; Britt, I.J.; Tung, M.A. Permeation of oxygen and water vapor through EVOH films as influenced by relative humidity. *J. Appl. Polym. Sci.* **2001**, *82*, 1866–1872.
29. Kim, D.; Kim, S.W. Barrier property and morphology of polypropylene/polyamide blend film. *Korean J. Chem. Eng.* **2003**, *20*, 776–782.
30. Takahashi, M.; Tashiro, K.; Amiya, S. Crystal structure of ethylene-vinyl alcohol copolymers. *Macromolecules* **1999**, *32*, 5860–5871.
31. Hernandez, R.J. Effect of water vapor on the transport properties of oxygen through polyamide packaging materials. *J. Food Eng.* **1994**, *22*, 495–507.
32. Buntinx, M.; Willems, G.; Adons, D.; Yperman, J.; Carleer, R.; Peeters, R. Evaluation of oxygen transmission rate and thickness before and after thermoforming mono- and multilayer sheets into trays with variable depth. In Proceedings of the 26th IAPRI Symposium on Packaging 2013, Espoo, Finland, 10–13 June 2013; pp. 386–398.
33. Buntinx, M.; Willems, G.; Adons, D.; Yperman, J.; Carleer, R.; Peeters, R. Impact of thermoforming on the oxygen transmission rate and thickness of thermoformed trays. In Proceedings of International Conference on Market Trends and Developments in Plastics Tubs, Cups and Tray Packaging, Cologne, Germany, 3–5 December 2013.
34. Jakobsen, M.; Jespersen, L.; Juncher, D.; Becker, E.M.; Risbo, J. Oxygen- and light-barrier properties of thermoformed packaging materials used for modified atmosphere packaging. Evaluation of performance under realistic storage conditions. *Packag. Technol. Sci.* **2005**, *18*, 265–272.
35. Rodriguez-Aguilera, R.; Oliveira, J.C. Review of design engineering methods and applications of active and modified atmosphere packaging systems. *Food Eng. Rev.* **2009**, *1*, 66–83.
36. Van Bree, I.; de Meulenaer, B.; Samapundo, S.; Vermeulen, A.; Ragaert, P.; Maes, K.C.; de Baets, B.; Devlieghere, F. Predicting the headspace oxygen level due to oxygen permeation across multilayer polymer packaging materials: A practical software simulation tool. *Innov. Food Sci. Emerg. Technol.* **2010**, *11*, 511–519.
37. Ragaert, P.; Vermeulen, A.; Buntinx, M.; Peeters, R. New research gives further insights on O₂-ingress in food packaging. *New Food* **2014**, *17*, 8–11.

© 2014 by the authors; licensee MDPI, Basel, Switzerland. This article is an open access article distributed under the terms and conditions of the Creative Commons Attribution license (<http://creativecommons.org/licenses/by/4.0/>).